

# A bolometric hyperspectral camera based on a birefringent interferometer for remote sensing in the thermal infrared

Matteo Corti<sup>1\*</sup>, Florian Zischka<sup>2</sup>, Fabrizio Preda<sup>3</sup>, Antonio Perri<sup>3</sup>, Dario Polli<sup>1,3,4</sup>, Giulio Cerullo<sup>1,3,4</sup>, Ondřej Ballada<sup>5</sup>, Cestmír Barta<sup>5</sup>, Lukáš Chroust<sup>5</sup>, Gianluca Valentini<sup>1,4</sup>, Ille C. Gebeshuber<sup>2</sup> and Cristian Manzoni<sup>4</sup>

<sup>1</sup>Politecnico di Milano, Dipartimento di Fisica, Piazza Leonardo da Vinci 32, I-20133 Milano, Italy

<sup>2</sup>Technische Universität Wien, Wiedner Hauptstrasse 8-10/134, 1040 Wien, Austria

<sup>3</sup>NIREOS S.R.L., Via G. Durando 39, 20158 Milano, Italy

<sup>4</sup>IFN-CNR, Piazza Leonardo da Vinci 32, I-20133 Milano, Italy

<sup>5</sup>BBT-Materials Processing Ltd., Doubická 11, 184 00 Prague 8, Czech Republic

**Abstract.** Remote sensing in thermal infrared bands (TIR) is largely dominated by cumbersome dispersive-type hyperspectral imagers, which usually require expensive and cryo-cooled quantum detectors to make up for their low optical throughput. Here, we present a compact and low-cost TIR hyperspectral camera based on the Fourier-transform approach. It combines an uncooled bolometer detector and a common-path birefringent interferometer made of calomel (Hg<sub>2</sub>Cl<sub>2</sub>). It features high optical throughput, an interferometric contrast greater than 90% even for incoherent radiation, spectral resolution tunable up to 4.5 cm<sup>-1</sup>, robust and long-term interferometric stability. Retrieving in a few minutes the infrared spectrum in all pixels of the TIR image, it could constitute a valuable tool for evaluating radiative cooling materials' spatial and spectral properties over extended areas. We test the capabilities of the instrument by measuring the emissivity map of different butterfly wings, which provide a natural example of radiative cooling.

## 1 Introduction

Hyperspectral imagers can be divided into two categories, according to the method used to collect the light spectrum in every pixel of the image.

With frequency-domain methods the light is filtered either spectrally, by using several bandpass filters, or spatially, coupling a slit to a prism/grating and sending the various wavelengths on different channels of an extended detector. The large optical losses introduced are usually compensated by high-sensitivity quantum detectors, such as mercury-cadmium-telluride (MCT) in the TIR. These are however expensive and require cryo-cooling to reduce thermal carriers generation.

In Fourier-transform (FT) systems, an interferometer splits the light into two delayed replicas and their interference signal is measured in each pixel as a function of the replicas delay. This produces an interferogram, whose FT yields the intensity spectrum of light according to the Wiener–Khinchine theorem. Compared to frequency-domain spectrometers, the FT method has prominent advantages: 1. higher signal-to-noise ratio for detector-dependent noise; 2. larger throughput, due to the absence of spectral or spatial filters; 3. more accurate and stable spectral calibration; 4. flexible spectral resolution, which can be adjusted by varying the total delay scan. These characteristics allow the use of lower detectivity thermal sensors, such as microbolometers, which are cost-effective, compact and do not require cooling [1].

However, to achieve high interferometric contrast and thus good spectral quality, the replicas' delay must be controlled with a precision of hundredths of the optical cycle and they must propagate collinearly toward the detector. Both of these requirements are challenging for remote sensing imagers, which often undergo strong vibrations and environmental perturbations. For example, typical amplitude-splitting interferometers like Michelson's are easily subjected to misalignments, as illustrated in Fig. 1(a), if not feedback-stabilized.

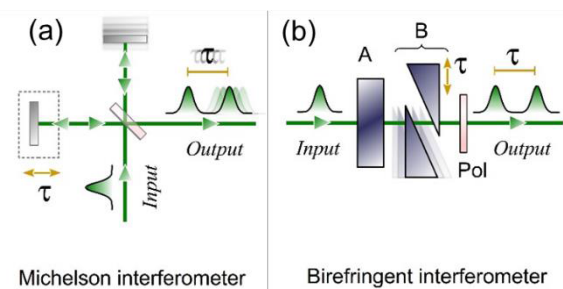


Fig. 1. Types of interferometers: (a) Michelson (b) TWINS.

## 2 TWINS interferometer

Recently, some of the authors have introduced and patented an innovative polarization-splitting interferometer, the Translating-Wedge-Based Identical Pulses eNcoding System (TWINS), which is based on the

\* Corresponding author: [matteo1.corti@mail.polimi.it](mailto:matteo1.corti@mail.polimi.it)

property that in a birefringent material ordinary and extraordinary light rays propagate with different velocities. The scheme of TWINS is shown in Fig. 1(b): it consists of a birefringent plate followed by two birefringent wedges with adjustable total thickness. The optical axes of the plate and the wedges are orthogonal, so that TWINS generates two field replicas whose relative delay can be precisely controlled by tuning the insertion of one of the wedges, mounted on a translation stage [2].

Since both field replicas follow the same optical path, they remain inherently collinear and their delay is locked with very high stability and reproducibility, decoupling external mechanical fluctuations without active stabilization. These characteristics make TWINS an ideal device for portable, on-field and spaceborne applications, as its footprint and weight are at least one order of magnitude smaller than standard amplitude-splitting interferometers.

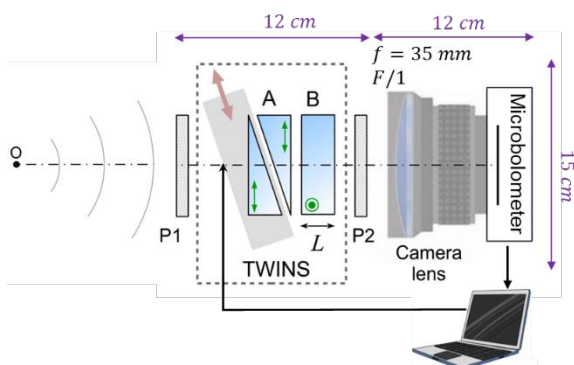


**Fig. 2.** Scheme of the hyperspectral camera. P1 and P2: linear polarizers, A and B: birefringent blocks.  $L = 5.9$  mm.

### 3 TIR hyperspectral camera

A hyperspectral camera based on TWINS was already implemented for the visible-NIR range [3]. To adapt it to the TIR, a calomel ( $\text{Hg}_2\text{Cl}_2$ ) interferometer, showing very large birefringence ( $\Delta n \approx 0.55$ ) and broad transparency range (0.4-20  $\mu\text{m}$ ), with light-collecting area  $15 \times 15$  mm<sup>2</sup>, was placed between orthogonal polarizers and coupled to an uncooled amorphous-silicon microbolometer detector with  $640 \times 480$  pixels (Fig. 2). The detection range of the sensor is limited to the 8-13  $\mu\text{m}$  range by a built-in bandpass filter; the imaging optics of the camera is a 35 mm, F/1 athermalized objective. The interferometric contrast was measured to be 97.6% with coherent light at

$\lambda = 9$   $\mu\text{m}$  from a quantum cascade laser (QCL) and 90.9% with the broadband incoherent light produced by an incandescent FeCrAl (Kanthal) filament. The maximum allowed spectral resolution, better than  $4.5$   $\text{cm}^{-1}$ , was retrieved from the longest possible scan of the interferometer wedges.

### 4 Imaging for Radiative Cooling

The capabilities of the instrument make it ideal for remote sensing in open environments but also for the characterization of radiative cooling materials. Since the dissipated heat scales linearly as the area, large surfaces of the plethora of materials continuously proposed need to be studied. Our camera enables a fast and accurate way to simultaneously characterize spatial and spectral properties of these materials.

To show the instrument capabilities, we characterized radiative exchange properties of different butterflies, which strongly depend on micro- and nanostructures on the wings [5]. Fig. 3(a) shows a wing of *Parthenos sylvia* in the visible, while Fig. 3(b) its emissivity map, spectrally integrated between 775 and 1325  $\text{cm}^{-1}$ . The image was generated from a spectral hypercube acquired with resolution of about  $25$   $\text{cm}^{-1}$ . Spectral emissivity curves of the circled regions, displayed in Fig. 3(c), show how emissivity changes both in spectral shape and intensity depending on the different areas of the wing.

### References

1. P. Griffiths, J. A. de Haseth, *Fourier Transform Infrared Spectrometry*, J. Wiley & Sons (2007)
2. D. Brida, C. Manzoni, G. Cerullo, *Opt. Lett.* **37**, 15 (2012)
3. A. Perri, B. E. N. de Faria, D. C. T. Ferreira, D. Comelli, G. Valentini, F. Preda, D. Polli, A. M. de Paula, G. Cerullo, C. Manzoni, *Opt. Exp.* **27**, 11 (2019)
4. A. Krishna, X. Nie, A. D. Warren, J. E. Llorente-Bousquets, A. D. Briscoe, J. Lee, *PNAS* **117**, 3 (2019)

**Fig. 3.** (a) Visible dorsal image of a *Parthenos sylvia* wing. (b) Emissivity map, spectrally integrated between 775 and 1325  $\text{cm}^{-1}$ . (c) Emissivity spectra of the circled regions in (b) acquired with spectral resolution of about  $25$   $\text{cm}^{-1}$ .

